



## 3D Simulation of Thermo-Hydraulic Enhancement of Flat-Plate Solar Collector Equipped with Twisted Tape

Fatima Zohra Bakhti<sup>1,2\*</sup> , Mohamed Si-Ameur<sup>2,3</sup> 

<sup>1</sup> Mechanical Department, Faculty of Technology, University of M'sila, 28000 M'sila, Algeria

<sup>2</sup> LESEI Laboratory, Avenue Chahid Boukhlouf Med Elhadi, 05000 Batna, Algeria

<sup>3</sup> Mechanical Department, Faculty of Technology, University of Batna 2, 05000 Batna, Algeria

\* Correspondence: Fatima Zohra Bakhti (fatimazohra.bakhti@univ-msila.dz)

Received: 08-18-2025

Revised: 10-19-2025

Accepted: 10-22-2025

**Citation:** F. Z. Bakhti and M. Si-Ameur, “3D simulation of thermo-hydraulic enhancement of flat-plate solar collector equipped with twisted tape ,” *Int. J. Energy Prod. Manag.*, vol. 10, no. 3, pp. 436–455, 2025. <https://doi.org/10.56578/ijepm100307>.



© 2025 by the author(s). Licensee Acadlore Publishing Services Limited, Hong Kong. This article can be downloaded for free, and reused and quoted with a citation of the original published version, under the CC BY 4.0 license.

**Abstract:** Flat plate solar collectors are widely employed in applications operating at low to moderate temperatures, including domestic water heating and various industrial uses. Their thermal performance is strongly influenced by the absorber tube, through which solar energy is transmitted to the circulating fluid. Conventional designs are often limited by low convective heat transfer, which has motivated studies on geometric enhancements to improve overall efficiency. The present work examines the thermo-hydraulic characteristics of a flat plate solar air collector fitted with twisted tape inserts having various twist ratios ( $\delta = 3, 4, 5, 6$ ), and compares the results with a plain tube collector. Air serves as the working fluid, and simulations were carried out over a Reynolds number range of 200–2000. A three-dimensional CFD approach was employed to study critical performance characteristics, including outlet temperature, Nusselt number, friction factor, pumping power, and thermal efficiency. The results show that twisted tape collector (TTC) provide considerably greater heat transfer compared to the plain collector (PC). At  $Re = 1000$ , the Nusselt number enhancement reached 35.19%, 44.55%, 50.15%, and 54.96% for twist ratios  $\delta = 6, 5, 4$ , and 3, respectively. Although this improvement is associated with increased pressure drops, the findings confirm that twisted tape inserts substantially enhance the heat transfer effectiveness of solar collectors by promoting turbulence and better fluid mixing.

**Keywords:** Flat plate solar collector; Thermal performance; Twisted tape; Heat transfer

### 1 Introduction

In recent years, solar energy has emerged as one of the cleanest, most sustainable, and widely recognized forms of renewable energy. Unlike fossil and nuclear resources traditionally used for power generation, including oil, natural gas, and coal, solar power provides a cleaner and more sustainable alternative, due to its vast availability, low environmental impact, and potential to transform energy systems. Although fossil fuels have significantly contributed to industrial progress, their limited availability and the emission of greenhouse gases and pollutants have made them major contributors to global climate change. The depletion of these resources and the urgency of environmental protection emphasize the need for the widespread implementation of renewable energy technologies. Among the various renewable alternatives, solar power distinguishes itself through its global abundance and advanced technological maturity, offering an effective pathway toward a sustainable and carbon-neutral energy future [1–3].

Solar energy finds practical use in different thermal applications, notably for heating air, water, swimming pools, and other thermal systems. A solar thermal system mainly comprises a solar collector, typically structured as an insulated metallic casing equipped with a transparent glazing (glass or plastic) and an absorber plate designed to capture solar radiation [4, 5]. The absorber receives the solar flux and converts it into heat, and subsequently transfers this energy to the thermal fluid circulating within tubes connected to its surface. Solar air collectors are especially attractive because they use air directly as the heat transfer medium, reducing cost, complexity, and maintenance requirements. These systems are widely applied in residential and commercial space heating, greenhouse warming, and drying agricultural products such as grains, fruits, and vegetables, as well as in humidification–dehumidification processes. The heat transfer efficiency of conventional solar air collectors is largely constrained by the low convective

interaction between the absorber surface and the airflow. This drawback arises from the poor thermophysical properties of air, which result in reduced thermal efficiency. To alleviate this drawback, a wide range of passive and active strategies have been developed to enhance thermal performance and heat transfer efficiency. These have been proposed to include the integration of fins serves to expand the heat transfer exchange surface, optimizing flow channel designs to enhance turbulence, and the introduction of turbulator elements such as twisted tape inserts [6–8]. Selecting a fluid with high thermal conductivity or high thermal capacity may also enhance heat transfer without necessarily increasing hydraulic losses. Among these passive methods, twisted tape inserts have demonstrated high effectiveness by generating secondary flow structures that intensify fluid mixing and thermal exchange without external energy input. Consequently, twisted tape configurations have been widely investigated both numerically and experimentally for their potential to enhance the performance of solar collectors [9–13].

## 1.1 Literature Review

Following the early success of Whitham [14] in demonstrating the potential of twisted tapes to enhance heat transfer, subsequent studies have made significant advancements to improve the thermal efficiency of tubes with various twisted tape geometries. Eiamsa-Ard et al. [15] carried out an extensive experimental study to examine the effects of the twist ratio and helical pitch of twisted tape inserts on the combined thermal and hydraulic performance of tube flows. Their results indicated that decreasing these geometric parameters enhanced heat transfer rates, but also increased pressure losses, resulting in a slight reduction in the overall thermal performance index. Similarly, Abolarin et al. [16] investigated the hydrothermal behavior of flows with twisted tape inserts arranged alternately in clockwise and counter clockwise directions under laminar, transitional, and turbulent flow regimes. In the turbulent regime, this alternating arrangement yielded a modest yet noticeable improvement in heat transfer compared to conventional twisted tape configurations.

Dalkılıç et al. [17] investigated turbulent flow in a tube equipped with a quad-channel twisted tape insert. Their experiments showed that raising the tape-to-tube length enhanced both heat transfer and flow resistance, while slightly reducing overall thermal performance. This effect was primarily attributed to fluid bypassing through the narrow gaps between the insert and the tube wall. Later studies substantiated these findings, showing that improvements in heat transfer are generally coupled with higher pressure losses. Singh et al. [18] analyzed turbulent flow enhancement in tubes equipped with circular and elliptical inserts featuring vertically oriented twisted tapes positioned at regular intervals. With rising Reynolds number, the system's overall thermal efficiency progressively diminished, because of the considerable rise in pressure drop that accompanied the higher Nusselt number.

Lopina and Bergles [19] experimentally demonstrated that twisted tape inserts behave similarly to fins in circular tube flows, resulting in an improvement in heat transfer of roughly 8–17%. The experimental findings indicated that the measured thermal transfer performance exceeded the predicted values by around 22.4%, mainly due to the introduction of a generalized correlation accounting for spiral flow effects. Eiamsa-Ard and Promvonge [20] conducted a comprehensive experimental study to assess heat transfer enhancement and flow resistance characteristics in ducts equipped with helical tape inserts. In the absence of a core rod, the average Nusselt number was found to increase by roughly 230% and 340%, respectively, relative to the smooth tube configuration. Zhang et al. [21] performed an experimental study to analyze the impact of twist ratios of 6, 7.5, and 10 on the thermo-hydraulic behavior of tubes equipped with twisted tape inserts. The outcomes demonstrated a 2.2–3.2-fold improvement in heat transfer performance, accompanied by a 13–14-fold rise in pressure drop relative to a smooth reference tube. Zhu and Chen [22] conducted a numerical study to explore thermal field enhancement within turbulent flow conditions utilizing single, double, and triple arrangements of twisted tape inserts. Their simulations revealed that these configurations increased flow resistance by approximately 6–21.2 times compared with a smooth tube, and that the resistance intensified with the number of tapes employed.

Fagr et al. [23] demonstrated that tapered twisted tapes in tubes provide thermal performance comparable to that of conventional tapes, suggesting that tape geometry can be optimized without a significant loss of efficiency. Building on the influence of tape configuration, Armbruster et al. [24] investigated periodically spaced twisted tapes in mixing devices to reduce fouling, showing that both tape length and arrangement affect fouling mitigation and energy efficiency. Extending the focus on geometric optimization, Piriyarungrod et al. [25] found that thermal efficiency of tapered tapes increases with the taper angle but decreases with higher twist ratios, highlighting the importance of design parameters. Man et al. [26] carried out experimental investigations showing that the twisted tape orientation and length, with emphasis on the anticlockwise arrangement in a concentric double-pipe heat exchanger, play a crucial role in determining thermal efficiency, in agreement with earlier findings on the optimal design of twisted tape inserts.

Feng et al. [27] investigated thermal flow characteristics of kerosene-based fuel flowing through tubes equipped with twisted tape inserts under supercritical pressure and found that these inserts greatly improved convective heat transfer by generating axial vortices mitigated buoyancy effects. Liao and Xin [28] conducted experiments on heat exchangers fitted with twisted tape inserts of varying twist ratios (5, 10, and 15) and different working fluids. The

results revealed that the configuration with the lowest twist ratio (5) exhibited the most efficient thermal behavior and the greatest friction factor, achieving performance improvements ranging from 2.46 to 4.70 times higher than those of smooth reference tubes.

In summary, although extensive research has demonstrated the benefits of twisted tape configurations employed to intensify heat exchange processes, limited attention has been given to their application in solar air collectors operating under laminar and transitional flow regimes. The present study aims to fill this research gap through a detailed three-dimensional CFD analysis of such systems.

## 1.2 Research Motivation and Objectives

A review of the literature shows that the use of twisted tape within a tube generates longitudinal vortices along the helical flow path, which intensifies turbulence and promotes fluid interaction, thereby improving thermal and mass transport. Twisted tape inserts have proven to represent an efficient passive approach for enhancing thermal performance in solar collectors; however, previous studies have shown that laminar and transitional flows yield more pronounced enhancements compared to turbulent regimes. Despite these promising findings, previous investigations have largely remained confined to laboratory-scale analyses and specific geometries, offering limited insight into the practical optimization of air-based solar collectors.

However, most of the existing studies have been primarily focused on liquid-based heat exchangers or turbulent flow conditions, leaving limited understanding of their applicability to solar air collectors operating under laminar regimes. Moreover, the combined effect of the twist ratio and Reynolds number on the overall thermo-hydraulic behaviour particularly the trade-off between improved thermal exchange and higher pressure losses remains insufficiently explored in the existing literature. This gap underlines the need for detailed numerical investigations to optimize solar collector performance using twisted tape inserts under realistic operating conditions.

Hence, the present work is specifically aimed at addressing these shortcomings by performing a comprehensive three-dimensional implicit finite volume numerical analysis of a flat-plate solar collector integrated with twisted tape elements, where air serves as the heat-transfer medium. The main objectives are to evaluate the influence of the geometric configuration of the twisted tape on the outlet air temperature and the collector's overall thermo-hydraulic efficiency. Particular emphasis is placed on exploring a wide Reynolds number range (200–2000), which corresponds to the laminar and early transitional flow regimes that are most relevant for practical solar air heating applications.

To quantify the enhancement obtained through the twisted tape configuration, key performance parameters outlet temperature, Nusselt number, friction factor, pumping power, and thermal efficiency were calculated and graphically compared with those of a plain collector.

The novelty of this study lies in its clear identification and exploration of the research gap concerning laminar airflow in solar collectors fitted with twisted tape inserts. This work offers an innovative approach that combines advanced numerical modelling with a geometric modification designed to promote swirl flow and disrupt the thermal boundary layer. While extensive research has been conducted on optimizing solar collectors, few studies have coupled three-dimensional CFD analysis with twisted tape geometries in air-type flat-plate collectors, making this investigation both novel and relevant. The twist in the tape is designed to enhance heat transfer by inducing secondary flows and improving mixing of the working fluid air within the collector. This approach distinguishes itself from conventional solar collector designs by introducing a turbulence-promoting element aimed at increasing the overall thermal efficiency.

Additionally, the study spans a broad range of Reynolds numbers (200–2000), providing a comprehensive assessment of the collector's performance under various flow conditions. This wide-range analysis enables a better understanding of the trade-offs between heat transfer enhancement and frictional losses, which is crucial for optimizing energy efficiency in practical systems.

By analyzing key performance metrics such as outlet temperature, Nusselt number, friction factor, and pumping power, the study not only quantifies thermal improvements but also evaluates the associated hydraulic penalties. The graphical representation of these results and their comparison with a plain solar collector's performance highlight the practical significance of the proposed design, offering valuable insights for future developments in compact, high-efficiency solar thermal systems.

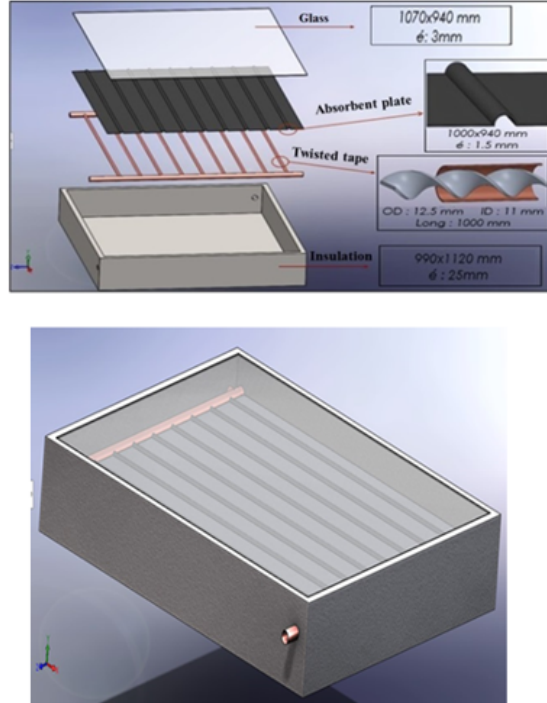
The structure of this paper has been organized to ensure a logical and coherent presentation of the research. Section 2 outlines the mathematical formulation, including the governing equations, boundary conditions, and details of the numerical procedure. Section 3 discusses the obtained results and examines the influence of twisted tape configuration and Reynolds number on the collector's thermo-hydraulic behavior. Finally, Section 4 summarizes the key outcomes and proposes potential directions for future work.

## 2 Mathematical Modelling

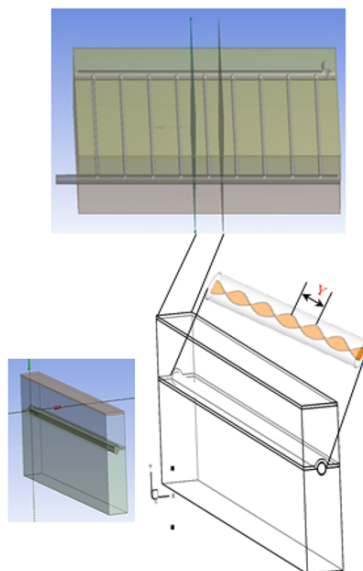
### 2.1 Configuration of the Geometry

Figure 1 depicts the geometry of the studied model, a flat-plate solar air collector with an effective area of  $1 \text{ m}^2$ . Air enters through the inlet manifold and is evenly distributed into nine parallel channels beneath a black-coated absorber plate, which captures solar radiation and transfers heat to the flowing air. The heated air is then collected in the upper manifold and discharged through the outlet.

The TTC has the same dimensions and design as the plain collector (PC). The TTC is equipped with twisted tape inserts made of copper, has a thickness  $e_T$ , a width  $W_T$  and has the same length  $L_T$  as the tubes. The strips are twisted through an angle of  $180^\circ$  to generate helical shapes characterized by twist ratios ( $\delta = Y/W_T$ ) of 3, 4, 5, and 6. Here,  $Y$  denotes the pitch length of the twisted tape, as shown in Figure 2.



**Figure 1.** 3D schematic of the flat plate solar collector



**Figure 2.** Illustration of the computational domain used in simulations

Table 1 presents the geometric details of the flat-plate solar collector, including the dimensions of the absorber plate, the configuration of the air channels, and the twisted tape parameters such as width, thickness, and twist ratio. These dimensions were selected based on typical configurations reported in previous studies [29], ensuring that the model represents realistic small-scale solar air heaters. The chosen geometry provides an optimal compromise between numerical efficiency and modeling accuracy allowing for a reliable assessment of thermo-hydraulic performance. To facilitate calculations and reduce calculation time, we selected a portion made up of a single tube (see Figure 2).

**Table 1.** Flat plate characteristics of the solar collector

Parameter	Value
Absorbent plate length, $L_a$	1000 mm
Absorbent plate width, $W_a$	120 mm
Number of riser tubes, $n$	9
Surface area of the collector plate, $S$	1 m <sup>2</sup>
Upper and lower header diameter, $D_{he}$	25.4 mm
Risers length, $L_R$	1000 mm
Risers internal diameter, $D_{RI}$	11 mm
Risers external diameter, $D_{RE}$	12.5 mm
Material of risers and twisted tape	Copper
Length of the twisted tape, $L_T$	1000 mm
Thickness of the twisted tape, $e_T$	0.3 mm
Width of the twisted tape, $W_T$	11 mm
Twist ratio of the tape, $\delta$	3, 4, 5, 6
Insulation material	Glass wool
Insulation length, $L_I$	100 mm
Insulation width, $W_I$	50 mm

The studied flat-plate solar collector is installed in the M'sila region of Algeria, with a latitude of 35°18' E, a longitude of 4°14' N, and thus can profit from the high solar intensity, during the summer for a date of June 20, 2024 at 1 p.m. with a 1 hour time difference.

- Material Properties

The thermophysical properties of the air, copper components (absorber tube and twisted tape), and the insulation material (glass wool) were extracted directly from the built-in material database of ANSYS Fluent. A detailed summary of these properties is provided in Table 2.

**Table 2.** Material properties used in the simulation

Parameter	Air	Copper	Glass Wool
$\rho$ (kg/m <sup>3</sup> )	1.225	8978	120
$C_p$ (J/kg·K)	1006.43	381	835
$k$ (W/m·K)	0.0242	387.6	0.038
$\mu$ (kg/m·s)	$1.7894 \times 10^{-5}$	—	—

## 2.2 Governing Equations

Initially, properties of the air ( $k$ ,  $\rho$ ,  $v$ ,  $C_p$ ) were considered temperature-dependent and were obtained from standard thermodynamic databases. However, the impact of using constant versus temperature-dependent fluid properties was examined. Our analysis confirmed that employing temperature-dependent properties resulted in negligible deviations in the Nusselt number predictions, thereby justifying the use of this assumption and the application of the Boussinesq approximation. Therefore, the following equations represent the conservation laws governing incompressible and steady convective flow within a Cartesian coordinate system [30–33]:

Mass Conservation Equation

$$\frac{\partial}{\partial x_i} (\rho u_i) = 0 \quad (1)$$

## Momentum Conservation Equation

$$\frac{\partial}{\partial x_i} (u_i u_j) = -\frac{1}{\rho} \frac{\partial p}{\partial x_i} + v \frac{\partial}{\partial x_j} \left[ \frac{\partial u_i}{\partial x_j} + \frac{\partial u_j}{\partial x_i} \right] \quad (2)$$

## Energy Conservation Equation

$$\rho C_p u_i \frac{\partial T}{\partial x_i} = k \frac{\partial}{\partial x_i} \left[ \frac{\partial T}{\partial x_i} \right] \quad (3)$$

### 2.3 Boundary Conditions

The resolution of the previously obtained system of equations requires the integration of boundary conditions for the governing equations in both cases: the plain and twisted collector configurations. The selection of boundary conditions, including inlet velocity, temperature, and heat flux, was based on experimental measurements conducted in the M'sila region of Algeria, ensuring that the chosen values accurately reflect real-world operating conditions. To evaluate the impact of these boundary conditions, a sensitivity analysis was performed by varying key parameters such as inlet velocity, absorber surface emissivity, and ambient temperature within realistic ranges. The results indicate that, while minor variations influence the outlet temperature, the overall heat transfer trends remain consistent, validating the robustness of the selected conditions.

- Inlet:

A velocity and temperature at the inlet (Velocity inlet):  $u_0, T_0 = 293.16$  K.

The mean inlet flow velocity is calculated using the Reynolds number.

$$Re = \frac{\rho u_0 D_h}{\mu} \Rightarrow u_0 = \frac{Re \mu}{\rho D_h}$$

where,  $D_h$  is the hydraulic diameter.

- Outlet (pressure outlet):

$$\begin{aligned} P &= P_{atm} \\ \frac{\partial T}{\partial x} &= \frac{\partial T}{\partial y} = \frac{\partial T}{\partial z} = 0 \end{aligned} \quad (4)$$

- The wall-fluid interfaces are coupled: (internal wall of the glass and air) and (interior wall of tube and fluid (air)):

$$k_w \frac{\partial T}{\partial n} \Big|_{\text{wall}} = k_f \frac{\partial T}{\partial n} \Big|_{\text{wall}} \quad (5)$$

- For the outer glass wall, a mixed limit condition is used to include radiation and convection heat transfer. There is a heat exchange by radiation between this surface and the sky.

Convective flow was calculated using Newton's law:

$$\varphi = hA (T_w - T_\infty) \quad (6)$$

The radiative heat transfer was modelled using the Solar Load Model for the M'sila region in Algeria, which is characterized by its specific climatic conditions. The operational conditions, including solar radiation intensity and ambient temperature, were selected to represent typical values for solar collector applications in this region. These parameters were chosen to accurately reflect real-world environmental conditions and to ensure the relevance of the simulation results. The solar radiation intensity was based on average daily values, while the ambient temperature was set according to seasonal variations observed in the M'sila area. This approach lets for an inclusive analysis of the system's performance under local environmental conditions.

## 2.4 Numerical Procedures

All 3D configurations were created using SolidWorks 2016 and analyzed in ANSYS Fluent v18.1, which applies a finite-volume-based numerical approach to compute the governing fluid flow and heat transfer equations. These equations were discretized using a second-order accurate scheme for convection terms, while the SIMPLE algorithm was used to link the velocity and pressure fields. The iterative solution process was initiated with the pressure field, and the pressure drop was efficiently computed using the continuity equation. Convergence was considered achieved when the normalized residuals reached  $10^{-6}$  for the energy equation and  $10^{-3}$  for the momentum and mass equations. To assess the impact of different numerical schemes on solution accuracy and stability, various discretization methods for convective terms were compared, including first and second order upwind, power-law and the QUICK scheme. Our analysis demonstrated that the second-order schemes offered the best balance between accuracy and computational cost. The selected scheme ensures numerical stability while minimizing artificial diffusion effects, thereby providing reliable and efficient results.

## 2.5 Grid Independence Study

Grid refinement tests were conducted to verify the consistency and robustness of the numerical results for all twisted tape designs. Multiple non-uniform grid distributions were examined to determine how mesh density affects the computed thermo-hydraulic parameters. The flow domain was discretized using a mixed-element mesh consisting of triangular and hexahedral cells, as shown in Figure 3. Finer elements were refined near the channel walls and around the twisted tape insert to resolve the swirl-induced flow structure and boundary layer effects accurately, while coarser elements were assigned to the central region to reduce computational time without compromising accuracy.

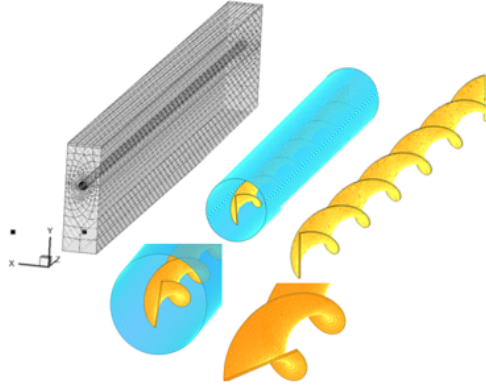


**Figure 3.** Mesh configuration

To assess mesh sensitivity, five different grid densities were generated for each twist ratio ( $\delta = 3, 4, 5$ , and  $6$ ). Simulations were carried out at  $Re = 1000$ , and the mean Nusselt number along with its variation ( $\Delta Nu$ ) were evaluated according to Eq. (7) [34]:

$$\Delta Nu\% = \left[ \frac{\overline{Nu} - \overline{Nu}_{ref}}{\overline{Nu}_{ref}} \right] \times 100 \quad (7)$$

The results are presented in Table 3 and depicted in Figure 4. The average Nusselt number was selected as the main evaluation parameter because it directly reflects the accuracy of heat transfer predictions.

**Table 3.** Variation of the Nu and  $\Delta Nu\%$  versus mesh nodes number for  $Re = 1000$

$\delta = 3$			$\delta = 4$			$\delta = 5$			$\delta = 6$		
Mesh	Nu	$\Delta Nu\%$									
568723	18.959	12.847	244184	16.987	15.936	244715	15.455	16.295	169520	14.649	29.63
590533	18.113	7.814	260920	16.192	10.510	261216	14.922	12.288	178539	14.134	25.07
606301	17.711	5.419	281126	15.637	6.722	278945	14.458	8.795	197136	13.569	20.068
631449	17.355	3.307	303726	15.399	5.098	341164	13.365	0.569	222878	12.931	14.426
668695	16.893	0.549	345441	14.775	0.839	404034	13.289	0	264620	12.227	8.192
737764	16.800	0	415299	14.652	0	—	—	—	333627	11.369	0.605
—	—	—	—	—	—	—	—	—	419203	11.301	0

As shown in Table 3 and Figure 4, the variation in the mean Nusselt number between successive mesh refinements decreases progressively as the grid is refined. A significant change in Nu is observed between the coarse and intermediate meshes, indicating that the flow and thermal gradients were not yet fully captured. However, for the two finest grids, the variation in the average Nusselt number becomes almost negligible less than 1% which confirms the numerical independence of the solution with respect to the mesh density.

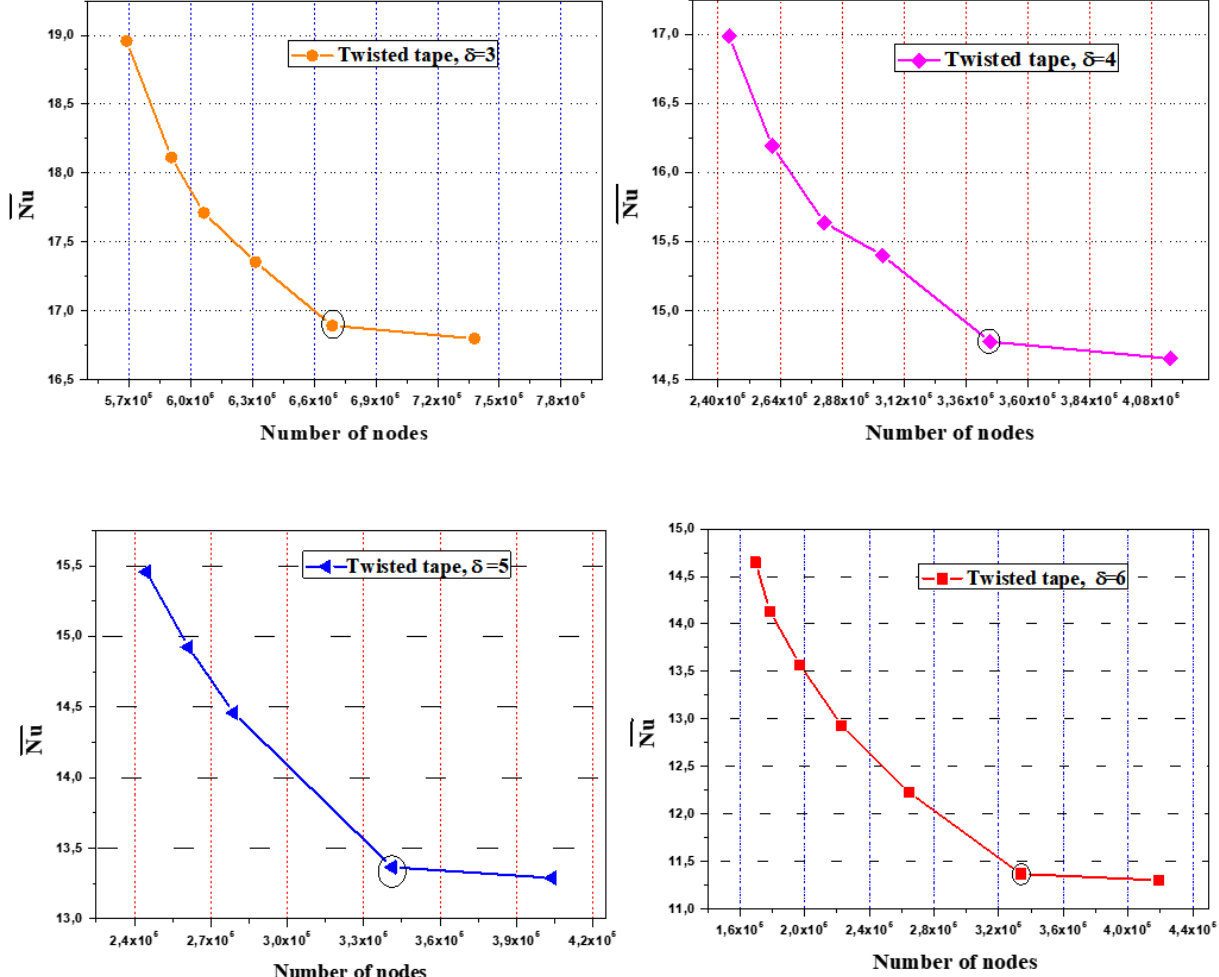


**Figure 4.** Nusselt number variation versus nodes number for the target four configurations ( $\delta=3, 4, 5, 6$ ) at  $Re = 1000$

As an illustration, for the configuration with a twist ratio of  $\delta = 3$ , Nu varies from 16.893 for 668,695 nodes to 16.800 for 737,764 nodes, corresponding to a relative change of approximately 0.55%. Similar trends are observed for  $\delta = 4, 5$ , and  $6$ , with variations of 0.84%, 0.57%, and 0.60%, respectively, between the two finest meshes. These results demonstrate that further refinement would not significantly affect the predicted thermal characteristics but would substantially increase computational time.

Based on this analysis, the following meshes were selected as optimal for the subsequent simulations:

- 333627 nodes for  $\delta = 6$
- 341164 nodes for  $\delta = 5$
- 345441 nodes for  $\delta = 4$
- 668695 nodes for  $\delta = 3$

These meshes ensure a good compromise between computational accuracy and efficiency. Hence, the adopted grid resolutions were used for all subsequent simulations.

## 2.6 Data Analysis

Several key performance metrics were derived from the outlet results, such as  $\Delta p$ ,  $\dot{m}$ ,  $T_{out}$ , and  $T_m$ . These quantities served to characterize both the heat transfer and fluid flow performance of the solar air collector,  $\Delta p$  represents the system's flow resistance and determines the power required to drive the air circulation, in reflects the

volume of air passing through the device, influencing the intensity of heat exchange. Meanwhile,  $T_{out}$ , and  $T_m$  were employed to quantify the overall thermal efficiency of the collector.

Collector's thermo-hydraulic performance was evaluated using total heat transfer rate, Nusselt number, friction factor, and pumping power.

The following dimensionless parameters and performance correlations employed to evaluate the thermo-hydraulic behavior of the solar collector, following standard definitions from the literatures [34–36].

- **Total heat transfer rate**

$$Q = \dot{m}C_p (\bar{T}_{out} - T_0) \quad (8)$$

where,

$\dot{m}$  is the mass flow rate;

$\bar{T}_{out}$  is the air outlet average temperature;

$T_0$  is the air inlet temperature.

- **Average convection heat transfer coefficient**

$$\bar{h} = \frac{Q}{A (\bar{T}_w - \bar{T}_m)} \quad (9)$$

where,  $\bar{T}_w$  and  $\bar{T}_m$  are respectively the wall and bulk average temperature.

- **Nusselt number**

$$\overline{Nu} = \frac{\bar{h}D_h}{k_f} \quad (10)$$

- **Enhancement of the Nusselt number**

The Nusselt number enhancement in the TTC compared to the PC is expressed as a percentage using the following relation:

$$\text{Enhancement } \overline{Nu}\% = \frac{\overline{Nu}_T - \overline{Nu}_p}{\overline{Nu}_T} \times 100 \quad (11)$$

where,

$\overline{Nu}_T$  is the twisted tape collector average Nusselt number;

$\overline{Nu}_p$  is the plain collector average Nusselt number.

- **Friction factor**

The pressure drop  $\Delta p$  across the test section of length L was used to determine the friction factor for the TTC and PC as follows:

$$f = \frac{1}{2} \frac{\Delta P}{L} \frac{D_h}{\rho U^2} \quad (12)$$

where,  $U$  is the air average velocity,  $\Delta p = P_o - P_{out}$ .

- **Pumping power (PP)**

$$PP = \Delta P \dot{V} \quad (13)$$

where,  $\dot{V}$  is the volume flow rate.

- **Thermal Efficiency**

The thermal efficiency of the solar air collector was computed using the following expression [37]:

$$\eta = \frac{\dot{m}C_p (T_{out} - T_o)}{IS} \quad (14)$$

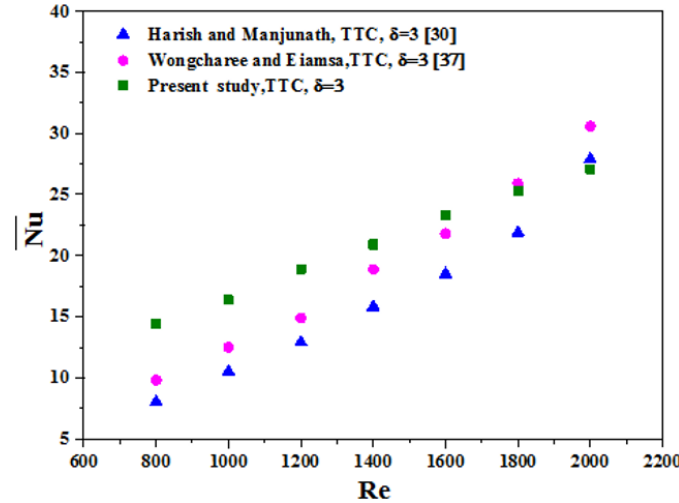
where,

$I$  is the intensity of solar irradiation received by the collector ( $\text{W/m}^2$ );

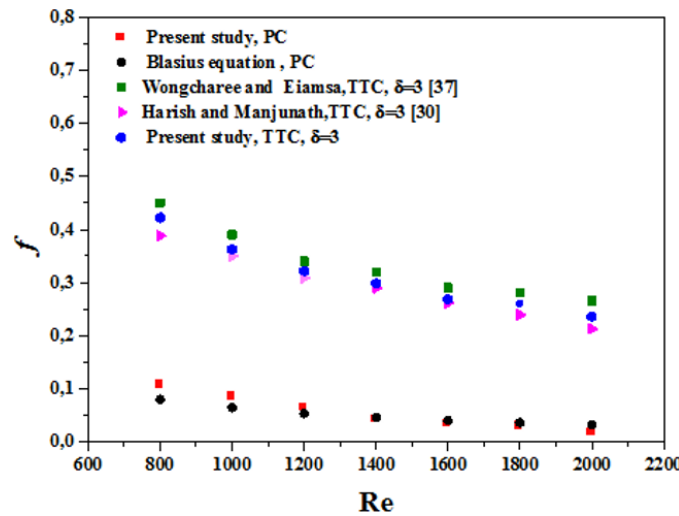
$S$  is the effective surface area of the collector ( $\text{m}^2$ ).

## 2.7 Numerical Simulation Validation

The accuracy of the proposed numerical model was assessed by evaluating the predicted Nusselt number and friction factor against established experimental data and theoretical models. Figure 5 illustrates a comparison between the current numerical predictions of the Nusselt number and the experimental measurements reported by Harish and Manjunath [30] as well as Wongcharree and Eiamsa-Ard [38]. This findings exhibited strong agreement, confirming the model's accuracy in predicting thermal characteristics.



**Figure 5.** Validation of the present numerical model: Comparison of computed and experimental average Nusselt numbers for the TTC case



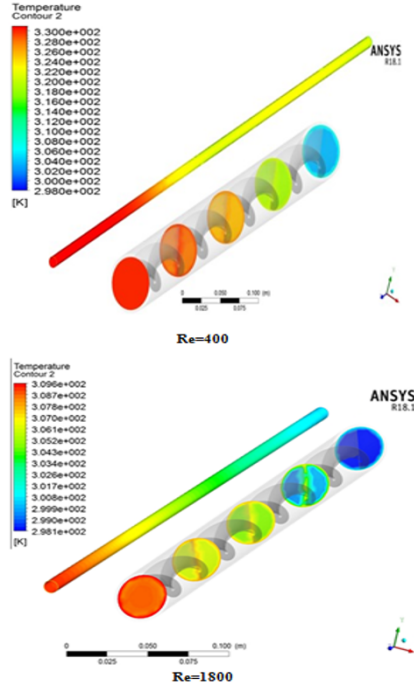
**Figure 6.** Validation of the numerical model: Comparison of computed and experimental friction factors for PC and TTC cases

Figure 6 presents the variation of the friction factor with Reynolds number for both configurations, exhibiting a decreasing trend that aligns with the classical Blasius correlation for smooth tubes. Our study's results for the plain collector closely follow this theoretical trend, confirming the accuracy of the numerical model. In the case of twisted tape inserts ( $\delta = 3$ ), the numerical results closely match the experimental findings of Harish and Manjunath [30] and Wongcharree and Eiamsa-Ard [38], further reinforces the reliability and accuracy of our approach. The decrease in friction factor with rising Reynolds number is consistent with the expected physical behavior, further validating the model's predictive capability. The consistency between our computational predictions and experimental findings underscores the model's validity and its utility in assessing similar solar collector configurations. This validation establishes the credibility of our model as a valuable tool for further investigations and design optimization in such thermal systems.

### 3 Results and Discussions

#### 3.1 Temperature Field and Flow Features

Figure 7 presents the temperature distribution at five cross-sections along TTC ( $\delta = 4$ ) for Re ranging from 400 to 1800. The results indicate that the temperature of the air decreases with an increase in Re, since the higher inlet velocity and mass flow rate that enhance heat removal. Along the tube, the temperature progressively increases and reaches its maximum near the outlet, reflecting continuous heat absorption during flow. This effect is more noticeable at lower Reynolds numbers, where the longer residence time promotes greater thermal exchange.



**Figure 7.** Temperature contours for  $\delta = 3$ : TTC

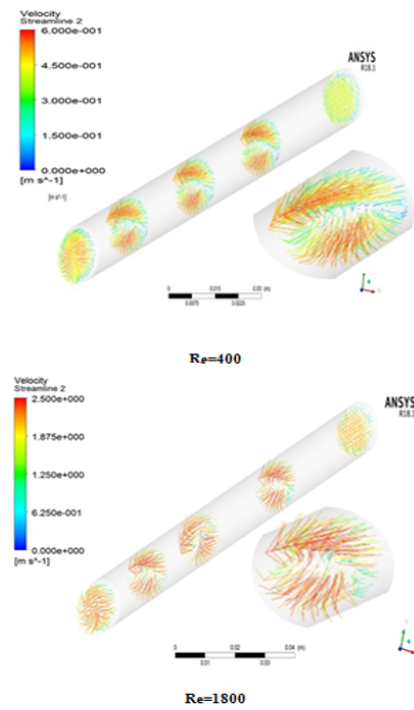


**Figure 8.** Vectors of the velocity for  $\delta = 3$ : TTC

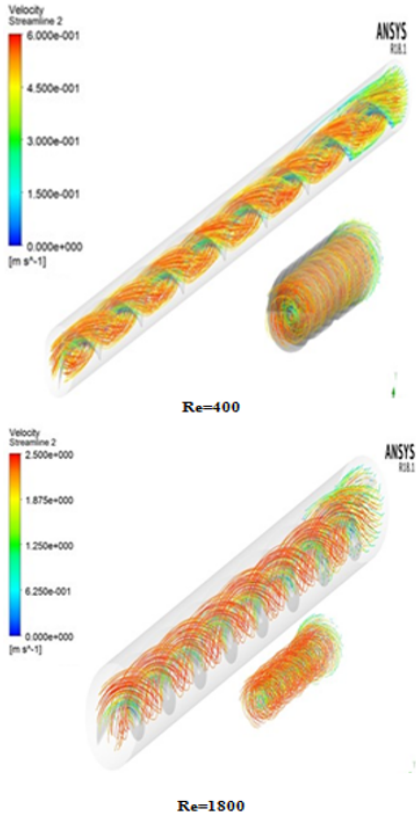


**Figure 9.** Pathlines of flow for  $\delta = 3$ : TTC

The figure also reveals that lower twisted ratios result in higher heat transfer rates and a greater outlet temperature. Such improvement results from the smaller twisted ratios induce better flow mixing and more intense cross-flows within the tube. As a result, these enhanced cross-flows disturb the thermal boundary layer and enhance the exchange of thermal energy between the fluid and the tube surface. In contrast, higher twisted ratios lead to a more uniform flow with reduced instabilities, resulting in less efficient mixing and a reduced heat transfer rate. Moreover, reduced twisted ratios enhance wall interactions, causing stronger velocity fluctuations that disturb the thermal layer and promote more efficient thermal exchange.

Figure 8 and Figure 9 illustrate the velocity vectors and pathlines of the fluid in the TTC ( $\delta = 4$ ) for Reynolds numbers  $Re = 400$  and  $Re = 1800$ , respectively. In both figures, the velocity vectors reveal that the inflow within the collector tube is uniform, reflecting a laminar flow regime at the entrance. As the fluid approaches the twisted tape, the direction of the velocity vectors deviates, reflecting the perturbation induced by the tape's shape. The fluid particles follow a spiral motion around the twisted tape, which induces an increase in turbulence and mixing within the flow. After passing around the tape, the velocity vectors come back to their initial direction after a short distance, confirming that the flow recovers its laminar characteristics post-tape.

It is noteworthy that the velocity profile and pathlines exhibit similar tendencies across both Reynolds numbers, albeit with noticeable differences in flow behavior. As the  $Re$  increases, the fluid accelerates, promoting faster flow and enhanced mixing. This increase in velocity explains the observed decrease in heat exchange in the collector, as the shorter residence time of the fluid at higher flow rates reduces the time available for efficient thermal exchange between the fluid and the collector surface. Increasing the Reynolds number accelerates the flow, reduces the thermal boundary layer thickness, and improves heat transfer at the fluid collector interface.

Figure 10 illustrates a comparison of the temperature difference  $\Delta T = T_{out} - T_0$  between the TTC (Twisted Tape Collector) and the PC (Plain Collector) in laminar regime. The findings clearly demonstrate that  $\Delta T$  decreases with rising of the  $Re$  indicating that higher flow rates reduce the temperature rise across the collector. This is due to the increased fluid velocity, which reduces the residence time and, consequently, the time available for heat transfer. Notably, the higher  $\Delta T$  in the TTC compared to the PC demonstrates the effectiveness of the twisted tape in improving convective heat transfer.

The addition of twisted tape results in a significant increase in the surface area available for heat exchange, which facilitates better fluid mixing and promotes a more effective convective heat transfer process. The twisted tape generates swirl flow that enhances fluid-wall interaction, improving heat transfer and yielding a higher outlet

temperature in the TTC than in the plain tube. The lowest twist ratio ( $\delta = 3$ ) achieves the highest outlet temperature due to stronger swirl and better fluid mixing, while higher twist ratios produce weaker swirl, less boundary layer disruption, and reduced heat transfer. This highlights the need to optimize the twist ratio for maximum thermal performance.

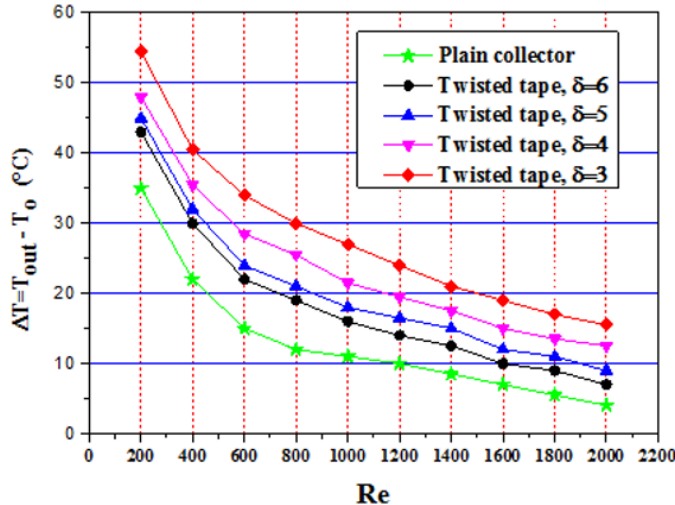


**Figure 10.**  $\Delta T$  Comparison at four twisted ratios: TTC and PC

Moreover, the observed decline in  $\Delta T$  with increasing Reynolds number further underscores the relationship between fluid velocity and heat transfer efficiency. As the Reynolds number increases, the fluid flow becomes more perturbed, which, although beneficial for mixing, can also lead to a decrease in the thermal boundary layer thickness, reducing the effectiveness of heat transfer in certain configurations. Therefore, there is a complex balance between flow instabilities, residence time, and heat transfer efficiency that must be considered when designing solar collectors.

### 3.2 Nusselt number

Figure 11 presents the relationship between the average Nusselt number and Reynolds number, along with the associated percentage enhancement, for the plain collector (PC) and twisted tape collector (TTC) under several twist ratios ( $\delta = 3, 4, 5$ , and  $6$ ). The comparative analysis reveals that the twisted tape collector (TTC) consistently achieves superior heat transfer performance compared to the plain collector (PC) across the entire range of Reynolds numbers. This improvement is mainly due to the secondary flow structures and vortex motion generated by the twisted tape, which enhance turbulence intensity and promote a more uniform temperature distribution along the flow channel. The inserts effectively disturb the main flow, breaking the thermal boundary layer and increasing the contact area between the fluid and the tube surface. As a result, the convective heat transfer rate is considerably improved for all examined twist ratios, confirming the effectiveness of twisted tape insert in enhancing the overall thermal performance of the collector.

The influence of the twisted tape ratio ( $\delta$ ) on the Nusselt number is clearly significant. As  $\delta$  decreases, the Nusselt number increases markedly, with the lowest twist ratio ( $\delta = 3$ ) providing the highest heat transfer rates. This improvement is attributed to the stronger swirling motion generated at smaller twist ratios, which intensifies turbulence, disrupts the thermal boundary layer, and enhances the overall heat exchange process. Conversely, larger twist ratios, such as  $\delta = 6$ , generate weaker swirl intensity and reduced turbulence, resulting in lower Nusselt number values and less efficient convective heat transfer. The numerical results confirm this trend, showing that the TTC with  $\delta = 3$  achieves the greatest enhancement, while the TTC with  $\delta = 6$  exhibits the poorest thermal performance. Therefore, optimizing the twist ratio is essential for maximizing the heat transfer efficiency of the collector.

The enhancement of the Nusselt number is influenced by both the twist ratio ( $\delta$ ) and the Reynolds number ( $Re$ ). As illustrated in Figure 11, the Nusselt number increases with rising Reynolds number, indicating that higher flow velocities promote stronger convective heat transfer. For example, at  $Re = 1000$ , the heat transfer enhancements for the twisted tape collectors are 35.19%, 44.89%, 50.15%, and 54.96% for  $\delta = 6, 5, 4$ , and  $3$ , respectively. This clearly demonstrates that smaller twist ratios result in greater heat transfer improvement. The results emphasize the strong interdependence between Reynolds number, twist ratio, and convective heat transfer performance in solar collectors. While higher Reynolds numbers enhance turbulence and thus improve heat transfer, the twist ratio remains a key geometric parameter that governs the intensity of swirl flow and boundary layer disruption. Therefore, achieving optimal thermal performance requires a proper balance between Reynolds number and twist ratio to maximize the heat transfer efficiency of the system.

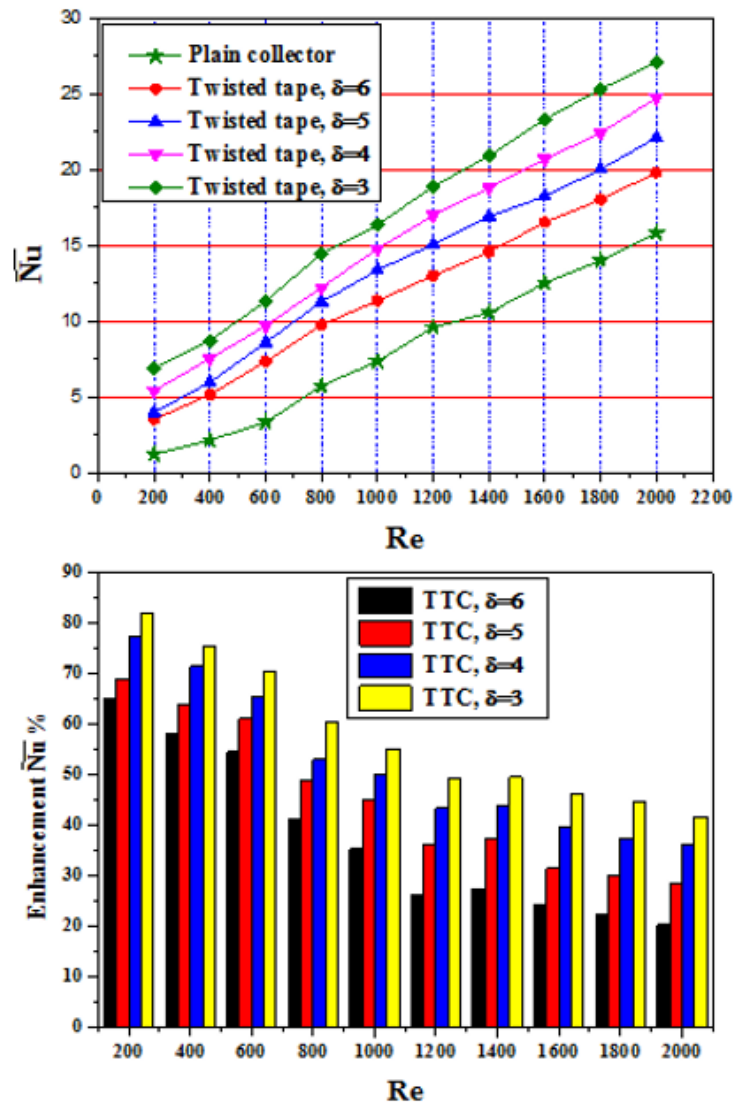


**Figure 11.** Average Nusselt number variation and its enhancement versus the Reynolds number

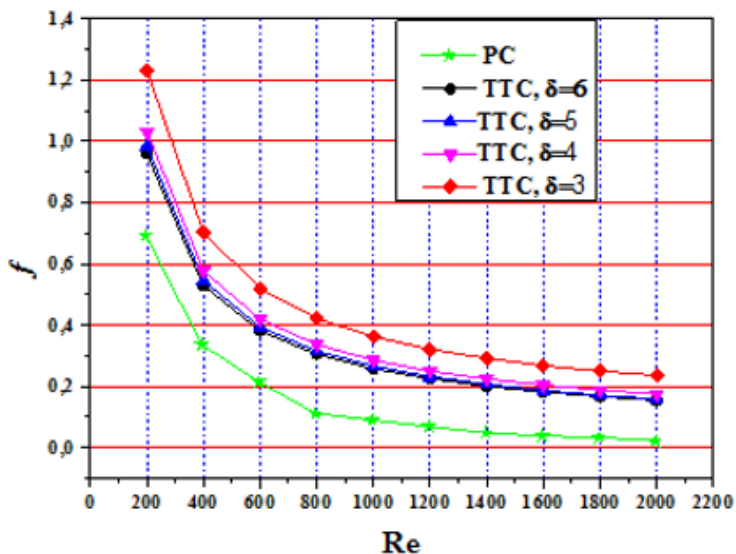


**Figure 12.** Friction factor comparison : TTC and PC

### 3.3 Friction Factor

Figure 12 presents the variation of the friction factor for the plain tube (PC) and the tube equipped with twisted tape collector (TTC). Overall, the friction factor decreases as the Reynolds number increases, showing a consistent trend across all cases. However, the TTC exhibits higher friction factors than the PC, with values decreasing as the twist ratio ( $\delta$ ) increases. Lower twist ratios, which generate stronger swirl intensity, produce higher friction factors, while larger  $\delta$  values reduce turbulence intensity and consequently decrease frictional resistance. At low Reynolds numbers, the influence of the twisted tape is more pronounced, leading to a noticeable rise in friction factor as the twist ratio decreases. In contrast, at higher Reynolds numbers, the effect of the inserts becomes less significant, and the friction factor values of the TTC gradually approach those of the PC. This behavior reflects the flow regime transition from laminar to turbulent conditions, where the interaction between the induced swirl and the main flow enhances convective heat transfer but simultaneously increases frictional losses.

The present findings highlight the critical role of the twist ratio ( $\delta$ ) in achieving this balance. A smaller twist ratio generates stronger swirl intensity and greater heat transfer enhancement but also leads to a substantial increase in pressure loss. Conversely, a larger twist ratio reduces turbulence intensity and pressure losses but limits the achievable heat transfer improvement. Hence, determining an optimal twist ratio is essential to maximize thermal efficiency while maintaining acceptable pumping power requirements.

### 3.4 Pumping Power

Figure 13 illustrates the variation in pumping power versus the Reynolds number for both PC and tubes with TTC at various twist ratio ( $\delta$ ). It is evident that the pumping power increases with the Reynolds number for all the cases under study. This increase is primarily due to the fact that, as the inflow velocity rises, the pressure drops also increases, requiring more power to overcome the resulting resistance and maintain the flow. Additionally, the results clearly indicate that the PC configuration requires higher pumping power than the TTC configuration. This can be explained by the fact that twisted tape collector create a disturbance in the flow, leading to increased chaotic flow and enhanced mixing, which increases frictional losses within the system.

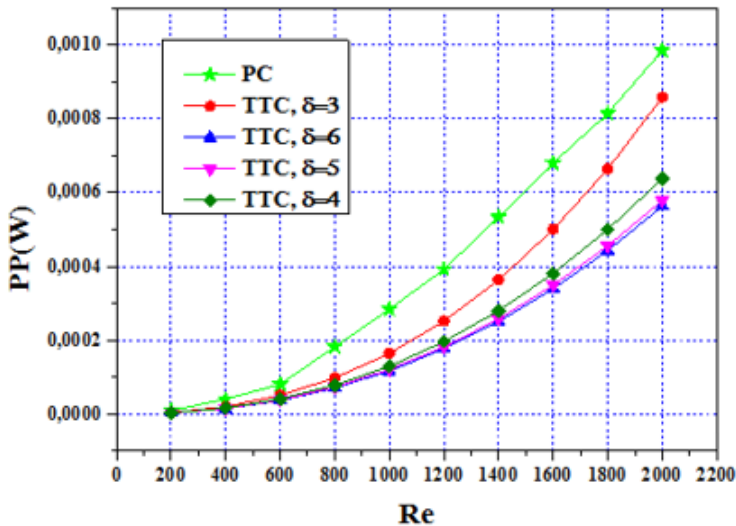


Figure 13. Pumping power comparison: PC and TTC

However, despite the increased friction, the twisted tape also improves heat transfer efficiency, which may offset the higher energy requirements in practical applications. Furthermore, the pumping power decreases as the twisted tape ratio increases, at least up to a certain point. This is due to the more effective flow redistribution and mixing that the twisted tape provides, which reduces the overall resistance compared to the plain tube. At higher twisted tape ratios, however, the increase in pumping power becomes more pronounced again. This suggests that there is an optimal twisted tape ratio, beyond which the additional frictional losses outweigh the benefits of improved heat transfer. Therefore, selecting an appropriate twist ratio is essential to achieve an effective balance between enhanced heat transfer and manageable pumping power.

The present findings highlight the critical role of the twist ratio ( $\delta$ ) in achieving this balance. A smaller twist ratio generates stronger swirl intensity and greater heat transfer enhancement but also leads to a substantial increase in pressure loss. Conversely, a larger twist ratio reduces turbulence intensity and pressure losses but limits the achievable heat transfer improvement. Hence, determining an optimal twist ratio is essential to maximize thermal efficiency while maintaining acceptable pumping power requirements.

### 3.5 Thermal Efficiency

The variations of thermal efficiency with Reynolds number for both the plain collector (PC) and twisted tape collector (TTC) configurations are shown in Figure 14. The results indicate that thermal efficiency increases with Reynolds number, as higher flow rates improve convective heat transfer and reduce thermal losses. Furthermore, TTC configurations consistently exhibit higher efficiencies than the PC, confirming the effectiveness of twisted tape inserts in enhancing energy performance. The configuration with the smallest twist ratio ( $\delta = 3$ ) provides the highest efficiency, attributed to stronger swirl flow and improved fluid mixing. However, the increase in efficiency is accompanied by a moderate rise in friction losses.

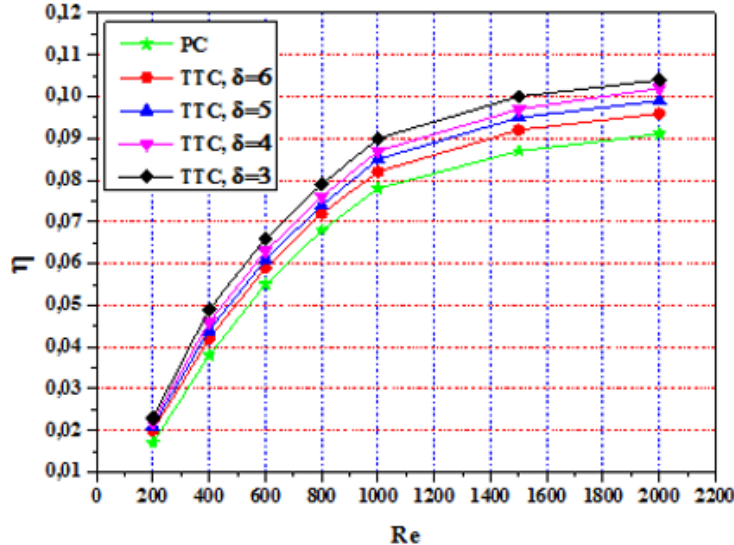


**Figure 14.** Thermal Efficiency comparison: PC and TTC

Overall, the inclusion of twisted tape turbulators significantly improves the thermal performance of the solar collector. The maximum efficiency enhancement reached approximately 10–15% compared to the plain collector under similar flow conditions.

### 4 Conclusion

This study evaluates the influence of twisted tape inserts on the thermal and hydraulic behavior of a flat-plate solar collector. Various twist ratios ( $\delta = 3\text{--}6$ ) are tested, and results are compared with a plain tube design. Using three-dimensional steady-state simulations in ANSYS Fluent, key parameters such as outlet air temperature, Nusselt number, friction factor, and pumping power are examined. Air flows with Reynolds numbers from 200 to 2000, capturing laminar and early transitional regimes. Findings highlight the role of tape geometry and flow conditions in enhancing overall collector efficiency.

The findings indicate that incorporating twisted tape inserts significantly improves the heat transfer of the solar collector relative to the plain tube setup. This improvement is primarily attributed to the induced secondary swirling flows, which enhance fluid mixing and weaken the thermal boundary layer. However, these benefits are accompanied by a rise in pressure drop, particularly for lower twist ratios and higher Reynolds number flows.

The key insights derived from this investigation can be summarized as follows:

- The twisted tape collector (TTC) exhibits higher outlet temperatures and Nusselt numbers than the plain collector (PC) for all values of  $Re$ .
- Decreasing the twist ratio ( $\delta$ ) enhances the heat transfer rate and the Nusselt number, with  $\delta = 3$  providing the best overall thermal performance due to stronger swirl generation.
- The percentage enhancement of  $Nu$  compared with the plain collector decreases from 54.96% to 35.19% as  $\delta$  increases from 3 to 6.
  - The friction factor is considerably higher for the TTC, although it decreases with both  $Re$  and  $\delta$ .
  - The pumping power is higher for the TTC due to increased pressure losses, but it remains within acceptable limits for the studied range.
- Overall, the twisted tape collector demonstrates the best configuration in terms of performance improvement, offering a favorable compromise between heat transfer enhancement and hydraulic penalty.

Unlike most previous studies that have primarily focused on liquid-based or turbulent flows, this work provides new insights into laminar air-flow behavior in solar collectors, offering a novel CFD-based understanding of swirl-induced thermal enhancement.

While the present study focused on steady-state flow conditions and a single geometric variable (the twist ratio), this choice was made to clearly isolate and understand its individual influence on the collector's thermo-hydraulic performance. The effects of variable solar radiation, radiation losses, and unsteady boundary conditions were not included in the current model, as they require separate treatment and significantly increase computational complexity. Future work will therefore aim to extend the model to include transient solar conditions, radiative heat exchange, and experimental validation, thereby strengthening the applicability of the present findings to real operating systems.

In practical terms, this study provides useful guidance for optimizing solar air collector design. The results help engineers select appropriate twist ratios that enhance heat transfer while maintaining reasonable pumping power, thereby improving system efficiency and reducing energy costs in applications such as solar drying and space heating.

In conclusion, the present study confirms that twisted tape inserts are an effective and low-cost passive technique for improving the performance of solar air collectors, particularly under laminar conditions. The results enrich the understanding of swirl-induced heat transfer mechanisms and provide valuable guidance for designing next-generation solar thermal systems that balance heat transfer enhancement with energy efficiency.

## Data Availability

The data used to support the findings of this study are available from the corresponding author upon request.

## Conflicts of Interest

The authors declare that they have no conflicts of interest.

## References

- [1] I. Luchnikov, D. Métivier, H. Ouerdane, and M. Chertkov, "Super-relaxation of space-time-quantized ensemble of energy loads to curtail their synchronization after demand response perturbation," *Appl. Energy*, vol. 285, p. 116419, 2021. <https://doi.org/10.1016/j.apenergy.2020.116419>
- [2] A. Ahmadi, M. A. Ehyaei, A. Doustgani, M. E. H. Assad, A. Hmida, D. H. Jamali, R. Kumar, Z. X. Li, and A. Razmjoo, "Recent residential applications of low-temperature solar collector," *J. Clean. Prod.*, vol. 279, p. 123549, 2021. <https://doi.org/10.1016/j.jclepro.2020.123549>
- [3] A. Raheem, W. Siddique, Z. H. Farooqui, T. Salameh, I. U. Haq, K. Waheed, and K. Qureshi, "Performance evaluation of adding helical-screw tape inserts in parabolic solar trough collectors as a source of cleaner energy production," *J. Clean. Prod.*, vol. 297, p. 126628, 2021. <https://doi.org/10.1016/j.jclepro.2021.126628>
- [4] J. Duffie and W. Beckman, *Solar Engineering of Thermal Processes*. New York: John Wiley and Sons, 1980.
- [5] S. A. Kalogirou, "Solar thermal collectors and applications," *Prog. Energy Combust. Sci.*, vol. 30, no. 3, pp. 231–295, 2004. <https://doi.org/10.1016/j.pecs.2004.02.001>
- [6] H. Hassan, S. Abo-Elfadl, and M. F. El-Dosoky, "An experimental investigation of the performance of new design of solar air heater (tubular)," *Renew. Energy*, vol. 151, pp. 1055–1066, 2020. <https://doi.org/10.1016/j.renene.2019.11.112>
- [7] A. Khanlari, A. Sözen, C. Şirin, A. D. Tuncer, and A. Gungor, "Performance enhancement of a greenhouse dryer: Analysis of a cost-effective alternative solar air heater," *J. Clean. Prod.*, vol. 251, p. 119672, 2020. <https://doi.org/10.1016/j.jclepro.2019.119672>
- [8] H. D. Ammari, "A mathematical model of thermal performance of a solar air heater with slats," *Renew. Energy*, vol. 28, no. 10, pp. 1597–1615, 2003. [https://doi.org/10.1016/S0960-1481\(02\)00253-7](https://doi.org/10.1016/S0960-1481(02)00253-7)
- [9] S. Eiamsa-Ard, P. Somkleang, C. Nuntadusit, and C. Thianpong, "Heat transfer enhancement in tube by inserting uniform/non-uniform twisted-tapes with alternate axes: Effect of rotated-axis length," *Appl. Therm. Eng.*, vol. 54, no. 1, pp. 289–309, 2013. <https://doi.org/10.1016/j.applthermaleng.2013.01.041>
- [10] W. Liu and B. Bai, "A numerical study on helical vortices induced by a short twisted tape in a circular pipe," *Case Stud. Therm. Eng.*, vol. 5, pp. 134–142, 2015. <https://doi.org/10.1016/j.csite.2015.03.003>
- [11] M. Rahimi, S. R. Shabanian, and A. A. Alsairafi, "Experimental and CFD studies on heat transfer and friction factor characteristics of a tube equipped with modified twisted tape inserts," *Chem. Eng. Process. Process Intensif.*, vol. 48, no. 3, pp. 762–770, 2009. <https://doi.org/10.1016/j.cep.2008.09.007>
- [12] S. Hasan and Z. H. Naji, "Augmentation heat transfer in a circular tube using twisted-tape inserts: A review," *J. Eng. Sustain. Dev.*, vol. 27, no. 4, pp. 511–526, 2023. <https://doi.org/10.31272/jeasd.27.4.8>
- [13] H. M. Hasan and M. H. Fagr, "Study of flow and heat transfer performance in the multi-configuration annulus twisted tube: A three-dimensional numerical investigation," *Int. J. Thermofluids*, vol. 23, p. 100728, 2024. <https://doi.org/10.1016/j.ijft.2024.100728>

- [14] J. M. Whitham, “The effect of retarders in fire tubes of steam boilers,” *Trans. ASME*, vol. 17, pp. 450–460, 1896. <https://doi.org/10.1115/1.4061126>
- [15] S. Eiamsa-Ard, K. Yongsiri, K. Nanan, and C. Thianpong, “Heat transfer augmentation by helically twisted tapes as swirl and turbulence promoters,” *Chem. Eng. Process. Process Intensif.*, vol. 60, pp. 42–48, 2012. <https://doi.org/10.1016/j.cep.2012.06.001>
- [16] S. M. Abolarin, M. Everts, and J. P. Meyer, “Heat transfer and pressure drop characteristics of alternating clockwise and counter clockwise twisted tape inserts in the transitional flow regime,” *Int. J. Heat Mass Transf.*, vol. 133, pp. 203–217, 2019. <https://doi.org/10.1016/j.ijheatmasstransfer.2018.12.107>
- [17] A. S. Dalkılıç, B. Uluç, M. S. Cellek, A. Celen, C. Jumpholkul, K. S. Newaz, and S. Wongwises, “Single phase flow heat transfer characteristics of quad-channel twisted tape inserts in tubes,” *Int. Commun. Heat Mass Transf.*, vol. 118, p. 104835, 2020. <https://doi.org/10.1016/j.icheatmasstransfer.2020.104835>
- [18] S. Singh, L. Pandey, H. Kharkwal, and H. Sah, “Augmentation of thermal performance of heat exchanger using elliptical and circular insert with vertical twisted tape,” *Exp. Heat Transf.*, vol. 33, no. 6, pp. 510–525, 2020. <https://doi.org/10.1080/08916152.2019.1662856>
- [19] R. F. Lopina and A. E. Bergles, “Heat transfer and pressure drop in tape-generated swirl flow of single-phase water,” *J. Heat Transf.*, vol. 91, no. 3, pp. 434–441, 1969. <https://doi.org/10.1115/1.3580212>
- [20] S. Eiamsa-Ard and P. Promvonge, “Heat transfer characteristics in a tube fitted with helical screw-tape with/without core-rod inserts,” *Int. Commun. Heat Mass Transf.*, vol. 34, no. 2, pp. 176–185, 2007. <https://doi.org/10.1016/j.icheatmasstransfer.2006.10.006>
- [21] Y. M. Zhang, J. C. Han, and C. P. Lee, “Heat transfer and friction characteristics of turbulent flow in circular tubes with twisted-tape inserts and axial interrupted ribs,” *J. Enhanc. Heat Transf.*, vol. 4, no. 4, pp. 297–308, 1997. <https://doi.org/10.1615/JEnhHeatTransf.v4.i4.50>
- [22] J. D. Zhu and H. Chen, “Numerical study on enhanced heat transfer by twisted tape inserts inside tubes,” *Procedia Eng.*, vol. 130, pp. 256–262, 2015. <https://doi.org/10.1016/j.proeng.2015.12.219>
- [23] M. H. Fagr, Q. A. Rishak, and K. S. Mushatet, “Performance evaluation of the characteristics of flow and heat transfer in a tube equipped with twisted tapes of new configurations,” *Int. J. Therm. Sci.*, vol. 153, p. 106323, 2020. <https://doi.org/10.1016/j.ijthermalsci.2020.106323>
- [24] S. Armbruster, F. Stockmeier, M. Junker, M. Schiller-Becerra, S. Yüce, and M. Wessling, “Short and spaced twisted tapes to mitigate fouling in tubular membranes,” *J. Membr. Sci.*, vol. 595, p. 117426, 2020. <https://doi.org/10.1016/j.memsci.2019.117426>
- [25] N. Piriyarungrod, S. Eiamsa-Ard, C. Thianpong, M. Pimsarn, and K. J. C. E. Nanan, “Heat transfer enhancement by tapered twisted tape inserts,” *Chem. Eng. Process. Process Intensif.*, vol. 96, pp. 62–71, 2015. <https://doi.org/10.1016/j.cep.2015.08.002>
- [26] C. Man, X. Lv, J. Hu, P. Sun, and Y. Tang, “Experimental study on effect of heat transfer enhancement for single-phase forced convective flow with twisted tape inserts,” *Int. J. Heat Mass Transf.*, vol. 106, pp. 877–883, 2017. <https://doi.org/10.1016/j.ijheatmasstransfer.2016.10.026>
- [27] S. Feng, X. Cheng, Q. Bi, H. Pan, and Z. Liu, “Experimental investigation on convective heat transfer of hydrocarbon fuel in circular tubes with twisted-tape inserts,” *Int. J. Heat Mass Transf.*, vol. 146, p. 118817, 2020. <https://doi.org/10.1016/j.ijheatmasstransfer.2019.118817>
- [28] Q. Liao and M. D. Xin, “Augmentation of convective heat transfer inside tubes with three-dimensional internal extended surfaces and twisted-tape inserts,” *Chem. Eng. J.*, vol. 78, no. 2–3, pp. 95–105, 2000. [https://doi.org/10.1016/S1385-8947\(00\)00134-0](https://doi.org/10.1016/S1385-8947(00)00134-0)
- [29] S. Jaisankar, T. K. Radhakrishnan, and K. N. Sheeba, “Experimental studies on heat transfer and friction factor characteristics of forced circulation solar water heater system fitted with helical twisted tapes,” *Sol. Energy*, vol. 83, no. 11, pp. 1943–1952, 2009. <https://doi.org/10.1016/j.solener.2009.07.006>
- [30] H. V. Harish and K. Manjunath, “Heat and fluid flow behaviors in a laminar tube flow with circular protruded twisted tape inserts,” *Case Stud. Therm. Eng.*, vol. 32, p. 101880, 2022. <https://doi.org/10.1016/j.csite.2022.101880>
- [31] F. A. Radhi, A. Ibrahim, A. Al Tarabsheh, A. A. Ali, H. L. Azeez, A. Fazlizan, and K. Sopian, “Experimental and numerical analysis of a solar collector enhanced by a square coil and a twisted tape,” *Case Stud. Therm. Eng.*, p. 106783, 2025. <https://doi.org/10.1016/j.csite.2025.106783>
- [32] A. Z. Sheshpoli, O. Jahanian, K. Nikzadfar, and M. A. Delavar, “Numerical and experimental investigation on the performance of hybrid PV / thermal systems in the north of Iran,” *Sol. Energy*, vol. 215, pp. 108–120, 2021. <https://doi.org/10.1016/j.solener.2020.12.036>
- [33] H. A. Ab Wahhab and A. H. Jassim, “Numerical analysis of horizontal geothermal heat exchanger at various burial depths for solar PV/T cooling in South Iraq weather,” *Int. J. Energy Prod. Manag.*, vol. 9, no. 4, pp. 267–273, 2024. <https://doi.org/10.18280/ijepm.090407>

- [34] F. Z. Bakhti and M. Si-Ameur, “A comparison of mixed convective heat transfer performance of nanofluids cooled heat sink with circular perforated pin fin,” *Appl. Therm. Eng.*, vol. 159, p. 113819, 2019. <https://doi.org/10.1016/j.applthermaleng.2019.113819>
- [35] F. Z. Bakhti, M. Si-Ameur, and B. Zerguine, “Enhancement of the cooling by mixed convection of a CPU using a rotating heat sink: Numerical study,” *Proc. Inst. Mech. Eng. E J. Process Mech. Eng.*, vol. 238, no. 1, pp. 144–157, 2024. <https://doi.org/10.1177/09544089221139110>
- [36] F. Z. Bakhti and M. Si-Ameur, “Elliptical pin fin heat sink: Passive cooling control,” *Int. J. Heat Technol.*, vol. 39, no. 5, pp. 1417–1429, 2021. <https://doi.org/10.18280/ijht.390503>
- [37] I. N. Rasool and R. S. Abdullah, “Experimental study of PV panel performance using backside water cooling chamber,” *Int. J. Energy Prod. Manag.*, vol. 8, no. 2, pp. 89–95, 2023. <https://doi.org/10.18280/ijepm.080205>
- [38] K. Wongcharee and S. Eiamsa-Ard, “Friction and heat transfer characteristics of laminar swirl flow through the round tubes inserted with alternate clockwise and counter-clockwise twisted-tapes,” *Int. Commun. Heat Mass Transf.*, vol. 38, no. 3, pp. 348–352, 2011. <https://doi.org/10.1016/j.icheatmasstransfer.2010.12.007>

## Nomenclature

$A$	Surface for thermal exchange, m <sup>2</sup>
$C_p$	Specific heat capacity, J/kg·K
$D_h$	Hydraulic diameter, m
$D_{he}$	Upper and lower header diameter, m
$D_{RI}$	Risers internal diameter, m
$D_{RE}$	Risers external diameter, m
$e_T$	Twisted tape thickness, m
$f$	Friction factor
$h$	Convective heat transfer coefficient, W/m <sup>2</sup> ·K
$I$	Solar radiation intensity, W/m <sup>2</sup>
$k$	Thermal conductivity, W/m·K
$L_a$	Absorbent plate length, m
$L_I$	Insulation length, m
$L_R$	Risers length, m
$L_T$	Twisted tape length, m
$\dot{m}$	Mass flow rate, kg/s
$n$	Number of risers
$\overline{Nu}$	Average Nusselt number
$P$	Pressure, Pa
$PP$	Pumping power, W
$\Delta P$	Pressure drop, Pa
$Re$	Reynolds number
$S$	Collector surface area, m <sup>2</sup>
$T$	Temperature, K
$T_0$	Inlet temperature, K
$\bar{T}_{out}$	Average outlet temperature, K
$\bar{T}_m$	Average bulk temperature, K
$\bar{T}_w$	Average wall temperature, K
$u_0$	Fluid inlet velocity, m/s
$\dot{V}$	Volume flow rate, m <sup>3</sup> /s
$W_a$	Absorbent plate width, m
$W_I$	Insulation width, m
$W_T$	Twisted tape width, m
$Y$	Twist tape pitch, m

## Greek symbols

$\delta$	Twisted tape ratio
$\eta$	Thermal efficiency
$\mu$	Dynamic viscosity, Pa·s
$\nu$	Cinematic viscosity, m <sup>2</sup> /s
$\rho$	Density, kg/m <sup>3</sup>
$\phi$	Total heat transfer, W

## Subscripts

atm	Atmosphere
f	Fluid
I	Insulation
o	Inlet
out	Outlet
m	Bulk
T	Twisted tape
w	Wall

## Abbreviations

CFD	Computational fluid dynamics
PC	Plain collector
TTC	Twisted tape collector